

Five vs Six Membered-Ring PAH Products from Reaction of *o*-Methylphenyl Radical and two C₃H₄ Isomers

Oisin J. Shields^{a#}, Matthew B. Prendergast^{a‡#}, John D. Savee^b, David L. Osborn^b,
Craig A. Taatjes^b, Stephen J. Blanksby^c, Gabriel da Silva^d, and Adam J. Trevitt^{a*}

^a Molecular Horizons and School of Chemistry and Molecular Bioscience, University of Wollongong, Wollongong, Australia, 2522

^b Combustion Research Facility, Sandia National Laboratories, Livermore, CA 94551-0969, USA

^c Central Analytical Research Facility, Queensland University of Technology, Brisbane, Australia, 4001

^d Department of Chemical Engineering, The University of Melbourne, Melbourne, Victoria, Australia, 3010

*adamt@uow.edu.au

O.J.S. and M. B. P. contributed equally to this work

‡ Current address: Department of Chemical Engineering, Massachusetts Institute of Technology, Massachusetts, 02139, USA

Abstract

Gas-phase reactions of the *o*-methylphenyl ($o\text{-CH}_3\text{C}_6\text{H}_4$) radical with the C_3H_4 isomers allene ($\text{H}_2\text{C}=\text{C}=\text{CH}_2$) and propyne ($\text{HC}\equiv\text{C}-\text{CH}_3$) are studied at 600 K and 4 Torr (533 Pa) using VUV synchrotron photoionisation mass spectrometry, quantum chemical calculations and RRKM modelling. Two major dissociation product ions arise following C_3H_4 addition: m/z 116 (CH_3 loss) and 130 (H loss). These products correspond to small polycyclic aromatic hydrocarbons (PAHs). The m/z 116 signal for both reactions is conclusively assigned to indene (C_9H_8) and is the dominant product for the propyne reaction. Signal at m/z 130 for the propyne case is attributed to isomers of bicyclic methylindene ($\text{C}_{10}\text{H}_{10}$) + H, which contains a newly-formed methylated five-membered ring. The m/z 130 signal for allene, however, is dominated by the 1,2-dihydronaphthalene isomer arising from a newly created six-membered ring. Our results show that new ring formation from C_3H_4 addition to the methylphenyl radical requires an *ortho*- CH_3 group – similar to *o*-methylphenyl radical oxidation. These reactions characteristically lead to bicyclic aromatic products, but the structure of the C_3H_4 co-reactant dictates the structure of the PAH product, with allene preferentially leading to the formation of two six-membered ring bicyclics and propyne resulting in the formation of six and five-membered bicyclic structures.

1. Introduction

Identifying the key chemical pathways responsible for the formation of fused-ring structures and polycyclic aromatic hydrocarbons (PAHs) is required to accurately model soot formation,¹⁻⁴ molecular weight growth in the interstellar medium⁵⁻⁶ and planetary atmospheres.⁷ For PAH formation, the progression from the first aromatic ring to bicyclic PAHs is an important step as this same ring-expansion process can be replicated to form increasingly larger PAHs.⁸⁻⁹ The production of bicyclic aromatics with fused “six-six” membered rings (e.g., naphthalene) versus “six-five” membered rings (e.g., indene) influences soot formation by changing the structural characteristics of the subsequent PAH products.^{1,10-12} Specifically, these six-five combinations introduce curvature into the PAH, whereas purely six-membered ring structures result in planar graphitic sheets. For phenyl radicals (C_6H_5), the textbook PAH formation process is the hydrogen-abstraction/ C_2H_2 -addition (HACA) framework, which leads primarily to six-membered ring formation,¹³⁻¹⁵ but this is just one contributing mechanism and it is recognized that further insights are required to better model the soot formation from the combustion of aromatic fuels – particularly involving branched aromatics (e.g., toluene, xylenes, trimethylbenzenes).

Toluene and other methylated benzenes are major components of typical gasoline fuel blends, often included in high concentrations (>30% v/v) due to their high energy density and anti-knock rating.¹⁶⁻¹⁷ Upon thermal activation, toluene will usually decompose by H atom loss, producing the resonance-stabilized benzyl radical ($C_6H_5CH_2$).¹⁷⁻²⁰ At high temperature conditions (>1200 K) other reactive intermediates, including the higher energy *o*-methylphenyl (*o*- $CH_3C_6H_4$) radical isomer, are also formed.²¹⁻²³ Although no direct detection of a methylphenyl radical has been reported from such environments, existing chemical models of combustion incorporate the

reactions of both benzyl and methylphenyl radicals.²⁴⁻²⁸ Additionally, through H atom or CH₃ loss, common during combustion, methylated and other functionalized PAHs could produce larger PAH analogues of the methylphenyl radical.²⁹⁻³⁰ Once generated these radical species can undergo subsequent reactions with other hydrocarbons leading to unique product channels. Chemical models of soot formation still struggle with aromatic fuels³¹ although there is significant ongoing progress in the area.^{26-27,31}

Previous studies on the *ortho*-methylphenyl radical (*o*-CH₃C₆H₄) + O₂ reaction demonstrated that, following O₂ addition, the *o*-methylphenyl peroxy (*o*-CH₃C₆H₄-OO) structure provides an accessible and labile H-atom for intramolecular abstraction by the neighboring peroxy group, ultimately leading to the characteristic products: *o*-quinone methide (*o*-CH₂=C₆H₄=O) + OH.³²⁻³⁴ Similar pathways are inaccessible for the *m*-methylphenyl (*m*-CH₃C₆H₄) and *p*-methylphenyl (*p*-CH₃C₆H₄) isomers. Cross-molecular beam single-collision experiments of *m*- and *p*-CH₃C₆H₄ radical reactions with C₃H₄ and C₄H₄ show that the methyl substituents are essentially spectators to the unimolecular rearrangements after adduct formation,³⁵⁻³⁸ but no study has investigated the effect of an *o*-methyl group on these or other hydrocarbon growth reactions.

To explore the possible ring-growth pathways of *o*-CH₃C₆H₄ with small hydrocarbons, we have observed its reactions with two C₃H₄ isomers: propyne (HC≡C-CH₃) and allene (H₂C=C=CH₂) using multiplexed photoionisation (PI) mass spectrometry at 600 K and 4 Torr. This synchrotron-based technique combines a flow reactor, time-of-flight mass spectrometry, and VUV photoionisation to enable the detection of reaction products with kinetic and isomeric resolution. We show that the addition reactions of *o*-CH₃C₆H₄ with allene and propyne result in both H atom

and CH₃ loss product pathways. Moreover, the major products of these reactions are seen to change depending on the C₃H₄ isomer, favoring the formation of a new six-membered ring for the allene case and a new five-membered ring for propyne. Reported reaction pathways are developed with quantum chemical calculations and Rice-Ramsperger-Kassel-Marcus master equation (RRKM-ME) rate theory, supporting our experimental product assignments and confirming the active role of the *ortho* methyl substituent.

2. Experimental

2.1 Multiplexed Photoionisation Mass Spectrometry

Gas-phase experiments were performed using multiplexed photoionisation mass spectrometry³⁹⁻⁴⁰ with VUV synchrotron radiation at the Chemical Dynamics Beamline,³⁸⁻⁴⁰ Advanced Light Source (ALS), Lawrence Berkeley National Laboratory, USA. The multiplexed photoionisation mass spectrometer comprises a quartz flow tube reactor, differentially pumped vacuum chamber, photoionisation source (*i.e.*, synchrotron radiation), and an orthogonal time-of-flight mass spectrometer as described in more detail elsewhere.³⁹⁻⁴⁰ A 650 μm diameter hole, positioned 37 cm along the tube, allows gas to continuously effuse from the quartz slow-flow reactor into a differentially pumped vacuum chamber. This gas is sampled by a skimmer to create a molecular beam that is intersected orthogonally by quasi-continuous vacuum-ultraviolet (VUV) synchrotron radiation and ions generated here are sampled by a 50 kHz pulsed orthogonal-extraction time-of-flight mass spectrometer. In the experiments described here, *o*-iodotoluene (*o*-CH₃C₆H₄-I), diluted in He, is photolyzed in the quartz flow tube at 248 nm by a pulsed KrF excimer laser (4 Hz, *ca.* 50 mJ cm⁻²), generating *o*-CH₃C₆H₄ radicals from carbon-iodine bond homolysis thus initiating the gas-phase radical chemistry.

All reactions considered here were conducted with the reactor maintained at 600 K and 4 Torr (533 Pa). The gas flow within the heated reactor was such that a reaction time of 0–50 ms could be monitored for a gas flow velocity of 4 m s⁻¹. The *o*-iodotoluene, C₃H₄ gas (either allene or propyne), and He gas was supplied to the reactor through separate mass-flow controllers resulting

in a combined flow rate of 50 sccm. The *o*-iodotoluene sample was entrained in He gas using a fritted bubbler with the liquid sample maintained at 19 °C (292 K) and under a pressure of 400 Torr (53 kPa). The resulting vapor pressure of *o*-iodotoluene was calculated to be 295 mTorr (39.3 Pa) at 292 K using Antoine parameters derived from Stull.³⁷ The number densities within the reactor at 600 K and 4 Torr were 6.2×10^{12} molecule cm⁻³ for *o*-iodotoluene, 2.1×10^{16} molecule cm⁻³ of either allene or propyne and 4.3×10^{16} molecule cm⁻³ for the He buffer gas. The total gas flow number density was 6.4×10^{16} molecule cm⁻³ at 600 K and 4 Torr.

All photoionisation data are normalized to the ALS photocurrent measured with a NIST-calibrated photodiode (SXUV-100, International Radiation Detectors Inc.). Ion signal acquired 20 ms before laser photolysis is averaged and subtracted from the post-laser signal so that positive ion signal is the result of ion signal created as a result of the laser photolysis. The PI spectra presented herein are the average of three individual acquisitions normalized over the integral of the spectrum. Mass spectra and kinetic traces represent the co-addition of at least three separate acquisitions of at least 900 laser pulses each.

For the 1,2-dihydronaphthalene reference PI spectrum, the purity of the sample was confirmed with conventional NMR and the spectrum was remeasured using a second commercial sample, finding no change in the spectrum (Figure S1).

2.2 Computational Chemistry

Reaction enthalpies and adiabatic ionization energies (AIEs) are calculated from electronic and zero-point energies computed in Gaussian 09.⁴⁵ All reaction enthalpies and barriers were calculated using the composite G3X-K method at 0 K.⁴⁶ The CBS-QB3 method⁴⁷⁻⁴⁹ was used to calculate AIEs and relative enthalpies for sets of 78 Da (C₆H₆), 116 Da (C₉H₈), and 130 Da (C₁₀H₁₀) isomers. Enthalpies are reported in kcal mol⁻¹ and AIE are reported in electron volts (eV). Both are calculated with 0 K electronic energies and include the zero-point energy correction. Stationary points were classified as either minima (no imaginary frequencies) or saddle points (one imaginary frequency). The assignment of a transition state between minima was verified by IRC calculations.⁵⁰

RRKM-ME analysis was performed on both reaction systems using the MultiWell 2020 software package.⁵¹⁻⁵³ Geometries, vibrational frequencies and calculated enthalpies for stationary points were taken from Gaussian 09 calculations, as described above, and internal degrees of freedom were approximated as either harmonic oscillators or hindered rotors. Hindered rotor potentials were determined using Fourier analysis of relaxed coordinate scans of the relevant rotor using a step size of 20°. Collisional energy transfer was modelled with the biexponential model $\Delta E_{\text{down}} = 200 \text{ cm}^{-1}$, as implemented in MultiWell 2020, using He as the collider. The Lennard-Jones parameters used for He were $\sigma = 2.5 \text{ \AA}$ and $\epsilon/k_B = 9.9 \text{ K}$, while Lennard-Jones parameters for all potential wells were set to $\sigma = 5.92 \text{ \AA}$ and $\epsilon/k_B = 410 \text{ K}$ (obtained from experimental results from toluene).⁵⁴ The energy grain was 10 cm⁻¹ for all calculations and the number of trials was 10⁷ for all simulations. Master equation simulations of these systems were performed at 600 K and 4 Torr, in accord with the experimental conditions.

3. Results and Discussion

3.1 Reaction Products

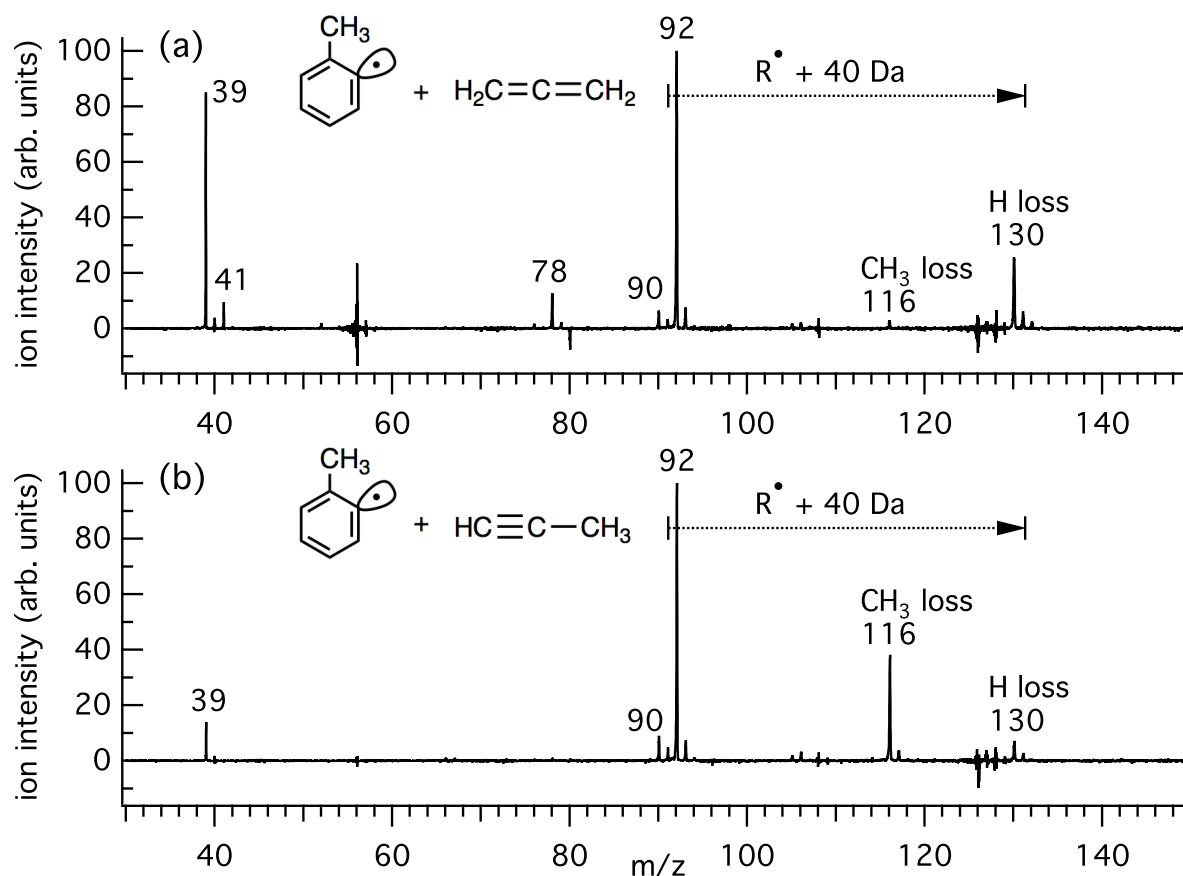


Figure 1. Mass spectrum at photoionisation energy 9.3 eV showing reaction products (integrated over 0–50 ms) following photolysis of *o*-iodotoluene in the presence of (a) allene and (b) propyne at 600 K and 4 Torr. Both mass spectra are normalized to the base peak. The base peaks at m/z 92 arise in large part from photolysis of the precursor and side reaction and not from the target reaction, as discussed in the text.

Photoionization (PI) mass spectra were recorded where 248 nm photolysis of *o*-iodotoluene was used to generate *o*- $\text{CH}_3\text{C}_6\text{H}_4$ radicals in the presence of (a) allene ($\text{H}_2\text{C}=\text{C}=\text{CH}_2$) or (b) propyne ($\text{HC}\equiv\text{C}-\text{CH}_3$) as shown in Figure 1. These mass spectra are integrated from 0–50 ms after photolysis, and acquired at a synchrotron photon energy of 9.3 eV with a reactor tube temperature

of 600 K. Within each spectrum, the ion signals at m/z 116 and 130 are attributed to reaction products of the *o*-CH₃C₆H₄ radical (91 Da) with C₃H₄ and correspond to C₃H₄ (+40 Da) addition with subsequent CH₃ loss (-15 Da) and H atom loss (-1 Da), respectively. These product signals were undetectable below 450 K, indicating temperature dependent kinetics, consistent with positive reaction entrance barriers. At 500 K the same products are detected, and these mass spectra are provided in the Supplementary Information (Fig S2). All analyses herein, however, relate to 600 K where stronger signal levels were recorded.

Based on the number density of allene and propyne in the reactor, *pseudo*-first order rate coefficients (k_{1st}) for m/z 116 and m/z 130 growth can (in the absence of a pseudo first-order analysis) be used to estimate an upper-bounds for the second-order rate coefficients for the title reactions under the 600 K and 4 Torr conditions. These estimates are $(2.3 \pm 0.3) \times 10^{-14}$ molecule cm³ s⁻¹ for *o*-CH₃C₆H₄ + allene and $(1.7 \pm 0.1) \times 10^{-14}$ molecule cm³ s⁻¹ for *o*-CH₃C₆H₄ + propyne (where uncertainties are simply 1 σ from the exponential fit). These values are similar in magnitude to the values predicted by Vereecken *et. al.* for phenyl + allene (5×10^{-14} cm³ molecule⁻¹ s⁻¹)⁵⁵ and phenyl + propyne (9×10^{-14} cm³ molecule⁻¹ s⁻¹) at 600 K.⁵⁶ Experiments performed at 421 K for phenyl + allene report the k_{2nd} at $(5.08 \pm 1.07) \times 10^9$ cm³ mol⁻¹ s⁻¹ (8.44×10^{-15} cm³ molecule⁻¹ s⁻¹).⁵⁷ These studies also predict that rates of H atom abstraction (i.e., C₆H₅ + C₃H₄ \rightarrow C₆H₆ + C₃H₃) will be at least an order of magnitude slower than radical addition at this temperature.⁵⁵⁻⁵⁶ The kinetic traces of all labelled ions in Figure 1 are included in the Supplementary Information (Figure S3 and Figure S4, Table S1) and this also assists with identifying species not relevant to the title reactions.

The mass spectra presented in Figure 1 are consistent with $C_{10}H_{10} + H$ and $C_9H_8 + CH_3$ comprising the major primary product channels from the $o\text{-CH}_3C_6H_4 + C_3H_4$ reactions and identifying these product isomers and the mechanisms leading to them is the main emphasis of this work (*vide infra*). However, a number of other products are identified in the mass spectra, which we first address briefly. Note that these products may arise from a number of processes, including side and secondary reactions, wall chemistry, photolysis, and dissociative photoionization.

For the allene case, side processes lead to the formation of m/z 39, 41 and 78 and this is based on their kinetic traces and fitted growth rates as shown in Figure S3 and Table S1. The m/z 39 signal is assigned as propargyl (C_3H_3), presumably a product of 248 nm allene photolysis. Propargyl is not a bimolecular reaction product, as the true reaction products at m/z 116 and m/z 130 have comparatively slower growth rates (Table S1). Although allene has a relatively low 248 nm absorption cross section⁵⁸ at 298 K, it likely has an elevated cross section at 600 K. It is known that propargyl recombines to form m/z 78 and this is in accord with the measured kinetic trace of m/z 78 (Figure S3).⁵⁹ The source of the m/z 41 signal is less clear, but its fast rise appears to indicate that it is related to the allene photochemistry (Figure S3, Table S1). Similarly, based on the kinetic trace (Figure S4) the m/z 39 signal in Figure 1 (b) appears to arise from side reactions, likely from the 248 nm photolysis of propyne.

Besides the addition channel for the $o\text{-CH}_3C_6H_4 + C_3H_4$ reactions, bimolecular products toluene (m/z 92) + propargyl (m/z 39) could be formed by a direct or indirect H-abstraction mechanism. Such a mechanism might be expected to proceed in minor amounts based on previous work on the phenyl radical.⁵⁵⁻⁵⁶ Unfortunately, here these m/z channels have interference from other processes.

We have shown previously that the photolysis of *o*-iodotoluene in the absence of other reactants gives rise to m/z 90 and 92;¹⁷ thus, the abstraction reaction is obscured in these experiments. However, experiments with isotopically labelled propyne- d_4 discussed later in the manuscript provide evidence that abstraction is only a minor channel.

Returning to the reaction products of the title reactions, it is evident from the ion intensities shown in Figure 1 that, following addition, H atom loss (m/z 130) is favored for the allene case and that CH_3 loss (m/z 116) is favored for propyne. At 9.3 eV the m/z 116:130 peak ratio for the propyne reaction is *ca.* 4:1 whereas the ratio is *ca.* 1:5 for the allene case. As discussed later this difference in branching ratio implies distinct mechanistic pathways between the two reactions, but first the isomeric assignments of m/z 116 and m/z 130 need to be considered.

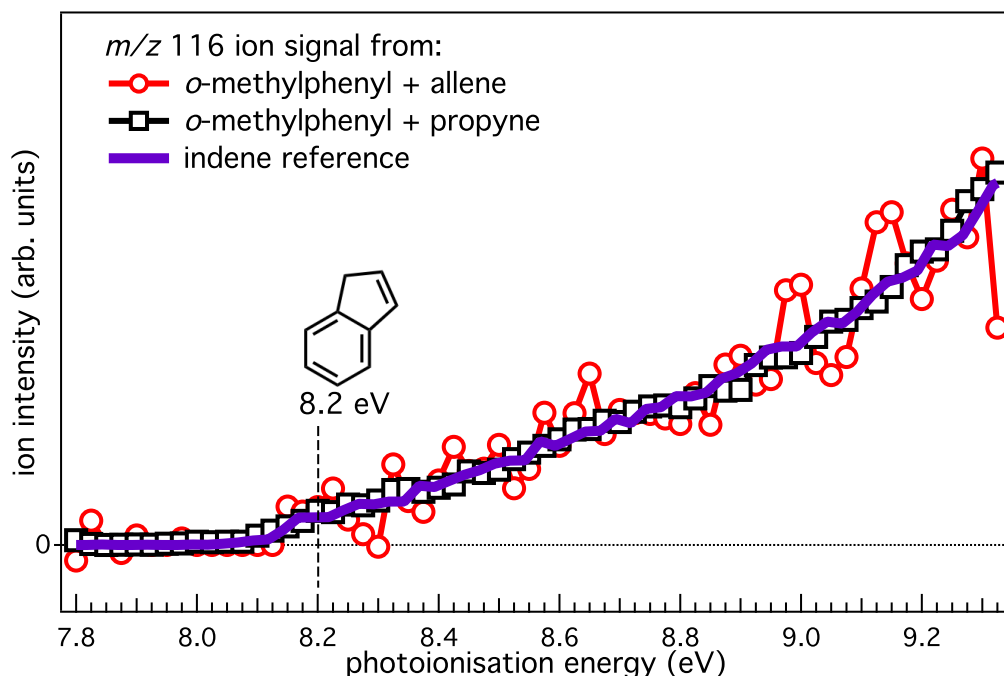
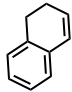
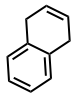
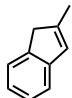
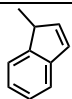
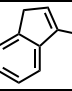
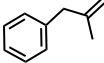
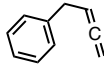


Figure 2. Photoionization spectrum of m/z 116 from $o\text{-CH}_3\text{C}_6\text{H}_4\text{+ allene}$ (circles) and $o\text{-CH}_3\text{C}_6\text{H}_4\text{+ propyne}$ (squares). A reference PI spectrum for an indene sample is shown (solid line) with the known AIE also indicated at 8.2 eV.

Figure 2 contains photoionization (PI) spectra associated with the m/z 116 signal from each reaction. Both of these traces are well matched to a reference PI spectrum for indene (C_9H_8 , 116 Da) acquired on the same instrument at 600 K. The match is very close for the propyne reaction, where indene is assigned as the primary reaction product, and the signal-to-noise ratio is superior to the allene reaction, where indene is formed in lower abundance. The PI signal onset at ~ 8.1 eV agrees with the calculated (8.2 eV) and literature (8.15 eV)⁶⁰ adiabatic ionization energy (AIE) for indene in Table S2. Other plausible isomers are ruled out on the basis of their ionization energy and relative stability (Table S2). This information leads us to conclude that indene is the sole m/z 116 isomer detected between 7.8–9.3 eV for both reactions.

For assignment of the m/z 130 product, there are several plausible candidates arising from H atom loss from the initial $C_{10}H_{11}$ adducts. The adiabatic ionization energy (AIE) values and relative enthalpies for a set of $C_{10}H_{10}$ isomers were calculated (Table 1) and out of these isomers, both 2-propynyl-toluene and 2-propadienyl-toluene are deemed unlikely as they have relative enthalpies 28 – 32 kcal/mol higher than the lowest energy $C_{10}H_{10}$ isomer, placing them near the energy of the reactants. However, based on relative stability the remaining $C_{10}H_{10}$ isomers (1,2-dihydronaphthalene, 1,4-dihydronaphthalene, 1-methylindene, 2-methylindene, and 3-methylindene) are all plausible candidates, with accessible reaction pathways (*vide infra*). Aside from 1,4-dihydronaphthalene (AIE = 8.6 eV), the candidate $C_{10}H_{10}$ isomers have ionization energies in the range of *ca.* 7.8 – 8.3 eV, complicating their discrimination.

Table 1. Calculated CBS-QB3 AIEs for $C_{10}H_{10}$ isomers (130 Da) and CBS-QB3 relative enthalpies (ΔH_f) are provided relative to the lowest energy isomer.

$C_{10}H_{10}$ isomer	Structures	Calculated AIE (eV)	Literature IE (eV)	Relative ΔH_f (kcal mol ⁻¹)
1,2-dihydronaphthalene		8.0	8.0 [61]	1.8
1,4-dihydronaphthalene		8.6	8.6 [63]	4.8
2-methylindene		7.8	-	0.5
3-methylindene		8.0	8.14 [62]	0.0
1-methylindene		8.0	8.27 [62]	1.5
2-propynyl-toluene		8.3	-	28.0
2-propadienyl-toluene		8.1	-	32.1

The m/z 130 PI spectrum obtained from each reaction is reported in Figure 3, along with measured reference spectra for 1,2-dihydronaphthalene (AIE = 8.0 eV) and 2-methylindene (AIE = 7.8 eV). Unfortunately, high-purity samples for 1,4-dihydronaphthalene, 1-methylindene, and 3-methylindene are difficult to acquire and so reference PI spectra for these isomers are unavailable. We also checked the PI spectrum of m/z 130 for both reactions at 500 K, compared with 600 K, and the traces are essentially the same (Figure S5).

Compared to the 1,2-dihydronaphthalene reference spectrum, the m/z 130 PI spectrum for allene tracks the reference spectrum well, including at the important onset region, but deviates at photon energies ≥ 8.6 eV. This deviation points to the presence of another isomer with a higher energy ionization onset and aligns with the AIE of 1,4-dihydronaphthalene (AIE = 8.6 eV in Ref. 63).

Thus, we tentatively assign the m/z 130 product signal from the o -CH₃C₆H₄ + allene reaction as a mixture of 1,2- and 1,4-dihydronaphthalene.

For the propyne case, the match of m/z 130 signal with the known spectrum for 1,2-dihydronaphthalene looks rather good at first pass. However, the experimental signal is above baseline between 7.8 and 8.0 eV, which is lower than the AIE of 1,2-dihydronaphthalene, suggesting the resemblance could be coincidental and/or there are other isomers present. The calculated AIE for 2-methylindene (7.8 eV) matches the earlier onset for the m/z 130 PI spectrum of o -CH₃C₆H₄ + propyne, as seen in the magnified inset to Figure 3. Although the m/z 130 PI spectrum for propyne diverges from the 2-methylindene reference spectrum at around 8.0 eV, this could result from the onset due to the presence of 1-methylindene and/or 3-methylindene (both AIE = 8.0 eV). Therefore, we assign the m/z 130 product signal for this reaction as a mixture of 2-methylindene and one or more other isomers.

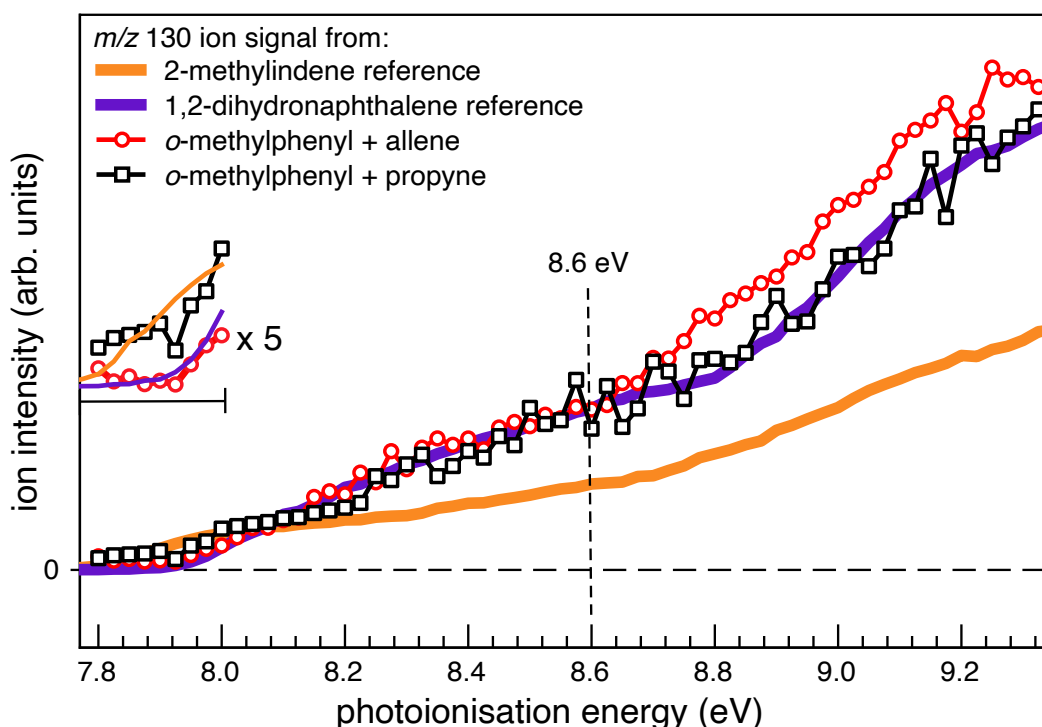


Figure 3. Photoionization spectrum of m/z 130 from $o\text{-CH}_3\text{C}_6\text{H}_4$ + allene (circles) and $o\text{-CH}_3\text{C}_6\text{H}_4$ + propyne (squares). A reference PI spectrum for 1,2-dihydronaphthalene (solid purple line) and 2-methylindene (solid orange line) are shown. The known AIE for 1,4-dihydronaphthalene is indicated at 8.6 eV.

In summary, signal at m/z 116 can be conclusively assigned as indene for both studied reactions. Assignment of products at m/z 130, however, is less certain. For $o\text{-CH}_3\text{C}_6\text{H}_4$ + allene, where $\text{C}_{10}\text{H}_{10}$ + H is the major reaction channel, the reaction forms a mixture of 1,2-dihydronaphthalene and 1,4-dihydronaphthalene. However, these dihydronaphthalene isomers do not appear to be products of the $o\text{-CH}_3\text{C}_6\text{H}_4$ + propyne reaction, where $\text{C}_{10}\text{H}_{10}$ + H is a minor reaction channel. In this case, we assign 2-methylindene as a $\text{C}_{10}\text{H}_{10}$ product with contributions from some other isomer(s). Importantly, these are not unequivocal assignments however, but by comparing the two reactions it is clear that CH_3 loss to yield indene is favored for the propyne reaction whereas H atom loss to form dihydronaphthalene isomers is favored for the allene reaction. To develop a rationale for

these differences, and provide more insight into the product assignment, the reaction mechanisms are required and therefore the potential energy landscapes for both reactions will now be discussed.

3.2 Reaction Mechanisms

To develop a mechanism consistent with the experimental results, and in return provide insight into unresolved assignments of the product detection experiments, enthalpies for key intermediates and transition states were calculated for both *o*-CH₃C₆H₄ + allene and *o*-CH₃C₆H₄ + propyne reactions using the G3X-K method. From previous studies on *ortho*-substituted phenyl radical oxidation,³²⁻³⁴ we expect that the *ortho*-substituent will influence the mechanism and the final product distribution compared to the analogous phenyl + C₃H₄ reactions.

In the schemes reported below, **A** denotes stationary points from *o*-CH₃C₆H₄ + allene, **P** for reactions with propyne, and **C** for stationary points common to both C₃H₄ reactions. All 0 K enthalpies are reported in kcal mol⁻¹ relative to *o*-CH₃C₆H₄ + allene (**A0**). Starting with Figure 4, two adducts are formed from *o*-CH₃C₆H₄ + propyne (**P0**, -0.2 kcal mol⁻¹), with enthalpies at -40.7 kcal mol⁻¹ for adduct **P1** and -35.7 kcal mol⁻¹ for adduct **P2**. Isomerization between **P1** and **P2** is mediated by **P3** (-16.0 kcal mol⁻¹). If adduct **P1** is formed, rearrangement and decomposition leads to indene + CH₃ (**C4**) *via* first a 1,5-H atom shift (TS **P1**→**P4** -37.8 kcal mol⁻¹), then cyclisation (TS **P4**→**P5**, -30.1 kcal mol⁻¹) and finally CH₃ loss to form indene with a reaction enthalpy of -43.4 kcal mol⁻¹. Alternatively, from **P5**, H-atom loss can produce 2-methylindene + H (**C7**) *via* a transition state at -32.9 kcal mol⁻¹, which is 4.9 kcal mol⁻¹ higher in energy than TS **P5**→**C4**. This higher H atom loss barrier is consistent with the favored loss of CH₃ observed experimentally for *o*-CH₃C₆H₄ + propyne (Fig. 1). Adduct **P1** forms following the lower barrier for propyne addition and is therefore expected to be the major entrance channel, suggesting the *m/z* 130 product for the propyne case is 2-methylindene based on the exclusivity of the end product of this pathway. The direct H-atom abstraction from *o*-CH₃C₆H₄ produces toluene (**C6**) and the

propargyl radical at $-21.5 \text{ kcal mol}^{-1}$ but appropriate treatment of this abstraction pathway, and the barrier along this coordinate, would require a more detailed computational investigation that is outside the scope of this study. Experimentally we observe ion signals consistent with this H-atom abstraction mechanisms for both reactions (m/z 39 and m/z 92 in Figure 1), although, as discussed above, there are several side processes that will also produce these signals.

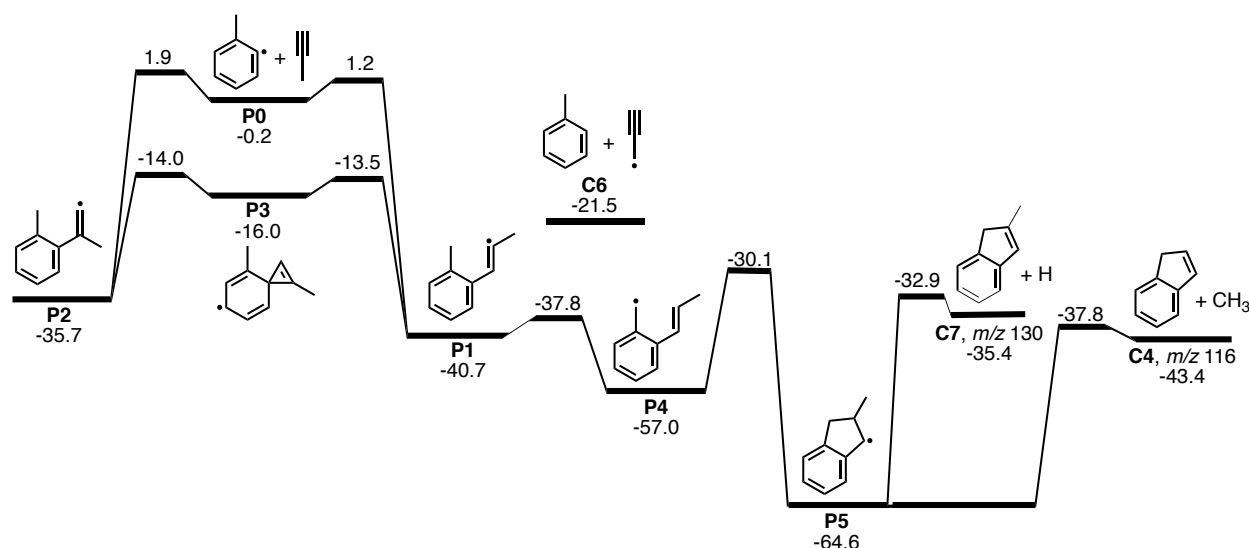


Figure 4. Potential energy schematic for the $o\text{-CH}_3\text{C}_6\text{H}_4 + \text{propyne}$ reaction starting at **P0**. Adduct formation and isomerization between adduct **P1** and adduct **P2** is included, and the remaining scheme follows the lowest addition barrier pathway via adduct **P1**. **P** denotes stationary points unique to $o\text{-CH}_3\text{C}_6\text{H}_4 + \text{propyne}$ and **C** stationary points common to both C_3H_4 reactions. G3X-K 0 K enthalpies reported in kcal mol^{-1} relative to $o\text{-CH}_3\text{C}_6\text{H}_4 + \text{allene}$ (A0).

To test the Figure 4 mechanism, the $o\text{-CH}_3\text{C}_6\text{H}_4 + \text{propyne}$ reaction was repeated with propyne- d_4 (44 Da) and the resulting PI mass spectrum is shown in Figure 5. Two products are detected at m/z 117 and 134 and, accordingly, the m/z 117 product ion (+1 Da shift from m/z 116) is consistent with CD_3 loss to form $\text{C}_9\text{H}_7\text{D}$ (and the small m/z 118 signal is the expected natural ^{13}C -isotopologue of $\text{C}_9\text{H}_7\text{D}$). The m/z 134 product is consistent with H loss from the adduct to form $\text{C}_{10}\text{H}_6\text{D}_4$. These pathways are included in the scheme in Figure 5 and in agreement with the mechanism in Figure 4. The lack of observed H/D scrambling indicates that these H/ CD_3 loss

mechanisms are rather direct, leaving little opportunity for H/D exchanges between the CH₃ group and the deuterated propyne chain.

Deuteration also allows us to monitor the direct H-abstraction pathway for this reaction as the D-abstraction from propyne-*d*₄ by *o*-CH₃C₆H₄ would generate singly deuterated toluene at *m/z* 93 (shifted away from the *m/z* 92 background signal). The signal at *m/z* 93 in Figure 5 is a mixture of the ¹³C-isotopologue of the background *m/z* 92 signal and the deuterated toluene adduct. Although the *m/z* 93 peak is not time resolved, the signal is 2.5% larger in ion intensity compared to the expected ¹³C-abundance of *o*-iodotoluene and this may point to a small product signal resulting from D-abstraction by *o*-CH₃C₆H₄. For the propyne case, the direct abstraction pathway appears to be minor under these conditions even accounting for the kinetic isotope effect in the labelling experiment.

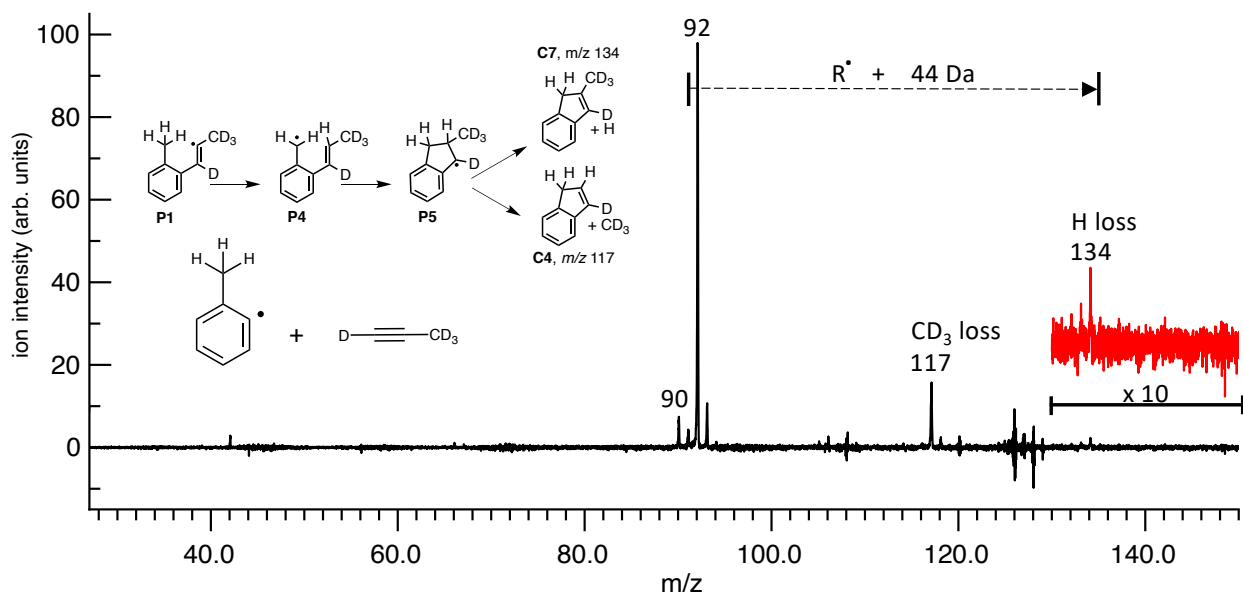


Figure 5. Product PI mass spectrum at 9.325 eV integrated over 0–50 ms after photolysis of *o*-iodotoluene in the presence of propyne-*d*₄ (44 Da) at 600 K. The ions at *m/z* 42 and 117 were assigned as isotopologues of the propargyl radical (C₃D₃) and indene (C₉H₇D). The mass spectrum is normalized to the base peak.

Returning to the calculations, now for the allene reaction, Figure 6 shows the formation of the two adducts from $o\text{-CH}_3\text{C}_6\text{H}_4$ + allene (**A0**) located at $-36.1\text{ kcal mol}^{-1}$ ($=\text{CH}_2$ addition, adduct **A1**) and $-59.1\text{ kcal mol}^{-1}$ ($=\text{C}=$ addition, adduct **A2**). Isomerization between adducts **A1** and **A2** is via **A3** ($-24.7\text{ kcal mol}^{-1}$). Pathways leading to the formation of 1,2-dihydronaphthalene + H (**A8**, $-34.6\text{ kcal mol}^{-1}$) and 1,4-dihydronaphthalene + H (**A9**, $-31.7\text{ kcal mol}^{-1}$) commence with a 1,5 H-atom shift via **TS A1** \rightarrow **A4** ($-24.1\text{ kcal mol}^{-1}$), the cyclisation from **A4** to form the 1,2,4-trihydronaphthalen-3-yl radical (**A5**, $-63.0\text{ kcal mol}^{-1}$) followed by subsequent H-atom loss forming either **A8** (1,2-dihydronaphthalene) or **A9** (1,4-dihydronaphthalene). Recall that from the experimental results in Figure 3, the m/z 130 PI spectrum for the allene reaction, the assignment of 1,2-dihydronaphthalene was based on the fit to a reference spectrum up to *ca.* 8.6 eV, where the deviation from the reference suggests the presence of the 1,4-dihydronaphthalene isomer. The production of both 1,2- and 1,4-dihydronaphthalene is supported by the mechanism in Figure 6, where pathways to both end products are accessible and competitive.

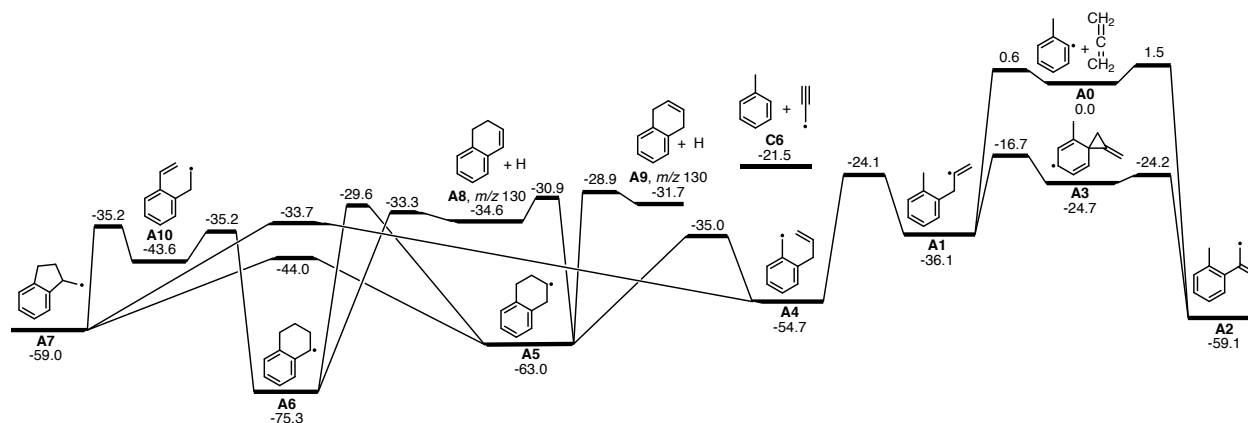


Figure 4. Potential energy schematic for the $o\text{-CH}_3\text{C}_6\text{H}_4$ + allene reaction starting from **A0**. Adduct formation and isomerization between adduct **A1** and adduct **A2** is included, and the scheme follows the lowest addition barrier pathway via **A1**. **A** denotes stationary points unique to the $o\text{-CH}_3\text{C}_6\text{H}_4$ + allene reaction and **C** stationary points common to both C_3H_4 reactions. G3X-K 0 K enthalpies reported in kcal mol^{-1} relative to $o\text{-CH}_3\text{C}_6\text{H}_4$ + allene (**A0**).

There are other pathways to these products. A cyclisation and rearrangement process from **A4** (**A4**→**A7**→**A10**→**A6**) or a 1,2-H atom shift from **A5** (**A5**→**A6**), forms the **A6** intermediate, which dissociates to exclusively form 1,2-dihydronaphthalene + H, which could add to the yield of 1,2-dihydronaphthalene relative to 1,4-dihydronaphthalene. Quantitative insight will come from the RRKM-ME calculations below, however even at this point it is apparent that the allene reaction pathways favor H atom loss, and this is in accord with the experimental results (Figure 1a).

Figure 7 shows the alternative addition pathways for propyne (adduct **P2**) and allene (adduct **A2**), which lead to a common intermediate (**C1**, $-58.2 \text{ kcal mol}^{-1}$) and so after this point the mechanism is shared. Cyclisation of **C1** produces **C2** ($-75.2 \text{ kcal mol}^{-1}$), *via* TS **C1**→**C2** ($-34.2 \text{ kcal mol}^{-1}$) then produces 1-methylindene + H (**C5**). Previous studies report that 1-methylindene and 3-methylindene readily isomerize at 600 K,⁶⁴⁻⁶⁵ so both isomers would result by this pathway in our experiment.

The 1-methylindene (**C5**) product is also formed from **C3** following a 1,2-H atom shift from **C2**. Alternatively, **C3** may eliminate CH₃ to form indene (**C4**). The likely rate limiting step for CH₃ loss is the **C2**→**C3** 1,2-H atom shift, which is 6 kcal mol^{-1} higher than direct H atom loss from **C2**. Therefore, indene + CH₃ production from **C1** is predicted to be minor, but non-zero, and is nevertheless assigned as the pathway responsible for the small indene + CH₃ signal observed for the allene experiments. Based on entrance barrier energetics, however, it is expected that flux through **C1** will be overall minor compared to the formation of either **P1** or **A1**.

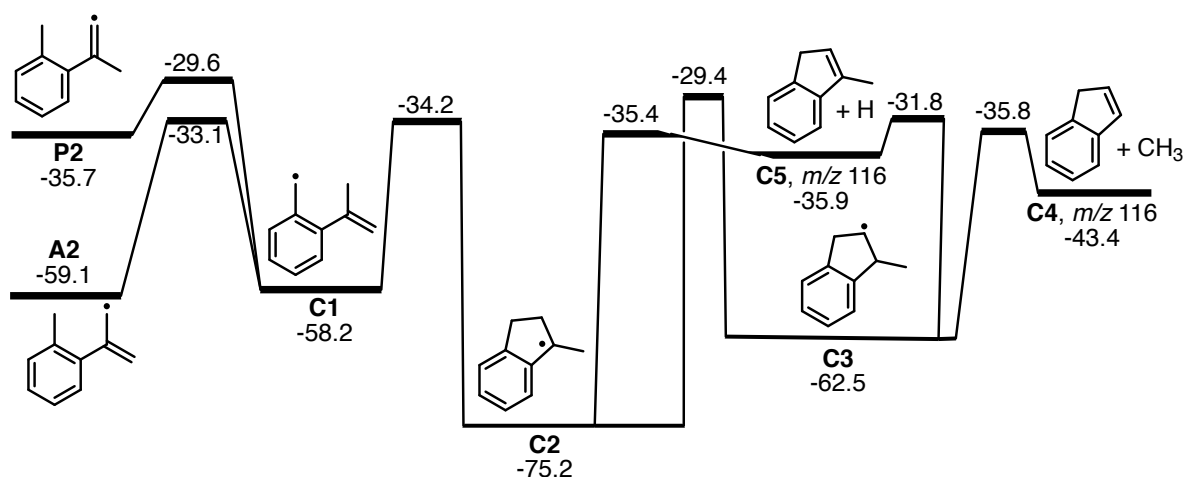


Figure 7. Potential energy schematic for isomerization between adduct **A2** and adduct **P2**. The reaction mechanism following the formation of the interconnected intermediate is identical after this point for both reactions. G3X-K 0 K enthalpies are reported in kcal mol⁻¹ relative to *o*-CH₃C₆H₄ + allene (**A0**).

Based on these potential energy schemes, the majority of the H atom loss product for the allene case is assigned as a mixture of 1,2-dihydronaphthalene and 1,4-dihydronaphthalene. As the potential energy scheme in Figure 7 shows, it is possible that some of the *m/z* 130 signal originates from the formation of 1-methylindene (and, as noted above, some subsequent thermal isomerization to 3-methylindene at 600 K), however, as 1-methylindene has a similar AIE to 1,2-dihydronaphthalene (both ~ 8.0 eV) this assignment cannot be verified experimentally. For *o*-CH₃C₆H₄ + propyne, the signal at *m/z* 130 (corresponding to H atom loss) is plausibly a combination of 1-, 2-, and 3-methylindene. The PI spectrum for *m/z* 130 does exhibit an onset at 7.8 eV, consistent with the AIE of 2-methylindene. No plausible mechanism leading to “six-six” bicyclic ring formation was identified for the *o*-CH₃C₆H₄ + propyne reaction. To extract more insight from these calculations, RRKM-ME modelling was performed using these stationary points.

3.3 RRKM Analysis

To improve on the predictions based on potential energy schemes, we examined the kinetics of both reactions with RRKM-ME simulations as implemented in the MultiWell program.⁵¹ These simulations predict branching ratios for each available product set, as well as the formation of stabilized C₁₀H₁₁ adducts. Two sets of model runs were required for each reaction, starting at each of the two initial adducts (adduct **P1** or adduct **P2** for the propyne case and adduct **A1** or adduct **A2** for the allene case – structures of these adducts are in Figure 4 and 6). As small errors in the enthalpies can result in large deviations in the predicted branching ratio, the G3X-K method was used for all stationary points.⁴⁶ An accurate method is particularly important for the reliable determination of key competing channels, such as between adduct **A1** and adduct **A2**. All stationary points in the simulation for each reaction are included in the Electronic Supplementary Information (Figures S6 and S7). The H-abstraction pathway was not included in these simulations. Table 2 lists the branching ratio results of these calculations depending on the starting adduct.

Table 2. Calculated product branching ratios for the reaction of *o*-CH₃C₆H₄ + propyne and *o*-CH₃C₆H₄ + allene at 600 K and 4 Torr. Simulated loss channels are also broken down into their respective product isomers – indene for CH₃ loss and 1-methylindene, 2-methylindene, 1,2-dihydronaphthalene and 1,4-dihydronaphthalene for H atom loss.

Starting Adduct	P1	P2	A1	A2
Fragmentation Channel	Branching Ratio (%)	Branching Ratio (%)	Branching Ratio (%)	Branching Ratio (%)
None (adduct)	10	0	6	0
H atom loss	2	98	94	96
1-methylindene	1	98	0	96
2-methylindene	1	0	0	0
1,2-dihydronaphthalene	0	0	58	0
1,4-dihydronaphthalene	0	0	35	0
CH ₃ loss	89	2	0	4
Indene	89	2	0	4

When **P1** is the starting adduct, the majority of product signal is predicted to be indene + CH₃ (89%), with a minor contribution originating from H atom loss (2%) – comprising 1-methylindene (1%) and 2-methylindene (1%). In contrast, simulations from adduct **P2** predict that CH₃ loss is minor (2%), and 1-methylindene + H will dominate (98%). When adduct **A1** is the starting point, no CH₃ loss product is predicted whereas H atom loss again dominates at 94%, comprising 1,2-dihydronaphthalene (58%) and 1,4-dihydronaphthalene (35%). Similar to adduct **P2**, branching from adduct **A2** has a minor contribution from CH₃ loss (4%) and H atom loss dominates with 1-methylindene and 3-methylindene products (96%).

To estimate the branching ratio for each reaction, the integrated densities of states for the corresponding transition states leading to adduct formation were compared at an activation energy of 18 kcal mol⁻¹ (the estimated internal energy of **A0** at 600 K). The result of this is that 72% of propyne addition leads to adduct **P1** and 28% to adduct **P2**, while 70% of allene addition forms adduct **A1** and 30% forms adduct **A2**. Absolute branching ratios were then determined by

normalizing the calculated branching ratios in Table 2 to the calculated partition between the two entrance channels for each reaction. The results for this comparison are shown in Table 3.

*Table 3. Calculated branching ratios for the o -CH₃C₆H₄ + propyne and o -CH₃C₆H₄ + allene reactions. Absolute branching ratios are estimated by partitioning the branching ratios for adduct **P1** and adduct **P2** or adduct **A1** and adduct **A2** based on the integrated densities of states for the transition states leading to the initial adducts.*

Fragmentation Channel	o -CH ₃ C ₆ H ₄ + Propyne Branching Ratios (%)	o -CH ₃ C ₆ H ₄ + Allene Branching Ratios (%)
None (adduct stabilized)	7	4
H atom loss	29	95
1-methylindene	28	29
2-methylindene	<1	0
1,2-dihydronaphthalene	0	41
1,4-dihydronaphthalene	0	25
CH ₃ loss	65	1
Indene	65	1

Overall, comparing the calculated branching ratios, the o -CH₃C₆H₄ + propyne reaction is predicted to produce indene + CH₃ in much higher yields compared to o -CH₃C₆H₄ + allene (65% vs 1%), consistent with the experimental findings. For the propyne case the predicted H atom loss branching ratio is 29% mostly arising *via* the formation of 1-methylindene (28%). A small portion of this H atom loss channel is predicted to form 2-methylindene (<1%). Therefore, the majority of the H atom loss products (m/z 130) from o -CH₃C₆H₄ + propyne are assigned as a mixture of 1-methylindene (and thus some 3-methylindene from thermal isomerization), while a smaller fraction is predicted to form 2-methylindene resulting in the onset at 7.8 eV as seen in Figure 3. In agreement with the assignment from section 3.2, RRKM-ME calculations for o -CH₃C₆H₄ + allene predict the majority of the H atom loss signal at m/z 130 originates from the formation of 1,2-dihydronaphthalene (41%). The 1-methylindene is the product with the next highest yield (29%), closely followed by 1,4-dihydronaphthalene (25%). Ideally, experimental branching ratios would

be in hand to compare with RRKM-ME calculations; however, this requires accurate photoionisation cross sections for each product isomer obtained from pure reference samples which are currently not available.

To summarize, the CH₃ loss channel (m/z 116) is assigned as indene for both reactions it is a major product for the propyne reaction and only a minor product in the allene reaction. The H atom loss channel (m/z 130) dominates for the allene case forming a mixture of 1,2-dihydronaphthalene, 1,4-dihydronaphthalene, and 1-methylindene. RRKM-ME simulations of this reaction indicate that 1,2-dihydronaphthalene is the dominant H atom loss product constituting 41% of the total ion signal. Combined with the predicted 1,4-dihydronaphthalene branching ratio (25%), these simulations suggest that 66% of products from the *o*-CH₃C₆H₄ + allene reaction form a new six-membered ring, a six-six bicyclic PAH. For the propyne reaction the H-atom loss channel is relatively minor, forming a mixture of 1-, 2-, and 3-methylindene. RRKM-ME simulations suggest that the 1-methylindene formation pathway dominates, although all of these products contain a new five-membered ring, these are six-five bicyclic PAHs. Therefore, it is clear that the allene + *o*-CH₃C₆H₄ reaction favors the formation of a new six-membered ring while for the propyne + *o*-CH₃C₆H₄ reaction, formation of a new five-membered ring instead dominates. A previous study investigating the reaction of *p*-CH₃C₆H₄ with allene and propyne found a shared general mechanism for both reactions: H loss to 6-methyl-1H-indene and 5-methyl-1H-indene.³⁵ Similarly, for the phenyl radical previous studies indicate that reactions with allene and propyne both produce indene as the major product.⁶⁶⁻⁶⁷ This difference in the present study directly results from the presence of the *ortho* methyl substituent, which alters the reaction mechanism and thus leads to distinct major products across both reactions. Together these results indicate that the molecular

configuration of the hydrocarbon reactant can alter the formation of the second aromatic ring and reinforces previous studies which suggested that an *ortho*-methyl substituent influences the reaction mechanism and changes the final product distribution.

4. Conclusions

VUV-synchrotron photoionisation mass spectrometry conducted at the ALS revealed two major product mass channels, m/z 116 and 130 from o -CH₃C₆H₄ radical reactions with allene and propyne consistent with CH₃ and H-atom loss and bicyclic ring formation. The m/z 116 product from both reactions is conclusively assigned to the bicyclic species indene (C₉H₈) by comparing experimental PI spectra to reference PI spectra for indene. Experiments with propyne-*d*₄ indicate the CH₃ fragment loss originates from the propyne reactant and the H fragment loss originates from the methyl substituent, supporting the calculated mechanisms. The m/z 130 product branching ratio differs for allene and propyne reactions and is favored for the allene case. For propyne reactions, m/z 130 signal is assigned to the formation of mostly 1-methylindene, while a small proportion of 2-methylindene formation results in the shifted onset of the m/z 130 PI spectrum for this reaction. On the other hand, the m/z 130 signal for the allene reaction is attributed to photoionisation of 1,2-dihydronaphthalene, 1,4-dihydronaphthalene, 1-methylindene, and 3-methylindene, although 1,2-dihydronaphthalene likely represents the dominant fraction of the product ion signal. Together these results suggest that the o -CH₃C₆H₄ + allene reaction favors the formation of a six-membered ring leading to fused “six-six” bicyclic rings, while the formation of a five-membered ring instead dominates for the o -CH₃C₆H₄ + propyne reaction leading to fused “six-five” bicyclic rings – thus demonstrating that by only changing the reactant isomer the branching ratio between five- and six-membered ring growth, one of the primary factors influencing PAH formation, can be altered.

5. Supporting Information

- Photoionisation spectra of second 1,2-dihydronaphthalene sample.
- Product mass spectra of allene + *o*-CH₃C₆H₄ and propyne + *o*-CH₃C₆H₄ at 600 K and 500K.
- Kinetic traces and derived first-order rate coefficients of major *m/z* channels for both reactions at 600 K.
- Calculated CBS-QB3 adiabatic ionization energies and relative enthalpies for possible C₉H₈ product isomers.
- Photoionisation spectra of *m/z* 130 for allene + *o*-CH₃C₆H₄ and propyne + *o*-CH₃C₆H₄ at 600 K and 500K.
- Complete potential energy schemes used for the RRKM-ME simulations of allene + *o*-CH₃C₆H₄ and propyne + *o*-CH₃C₆H₄.

6. Author contributions

The manuscript was completed with contributions of all authors. All authors have given approval to the final version of the manuscript.

7. Conflicts of interest

There are no conflicts to declare.

8. Acknowledgements

O. J. S acknowledges receipt of an Australian Government Research Training Program Scholarship. This work was supported by computational resources provided by the Australian Government through the National Computation Infrastructure under the National Computational Merit Allocation Scheme. The authors would also like to thank S. P. Sundar for assistance in generating and running the Multiwell simulations and Dr B. B. Kirk for assistance with experiments. The authors are grateful for the financial support of the Australian Research Council through the Discovery and Future Fellowship programs (DP170101596, DP140101237, DP130100862 and FT130101304). The participation of J. D. S., D. L. O., and C. A. T., and the development and operation of the MPIMS kinetics apparatus, are supported by the Office of Chemical Sciences, Geosciences, and Biosciences, Office of Basic Energy Sciences, United States Department of Energy. Sandia National Laboratories is a multi-mission laboratory managed and operated by National Technology and Engineering Solutions of Sandia, LLC, a wholly owned

subsidiary of Honeywell International, Inc., for the U.S. Department of Energy's National Nuclear Security Administration under contract DE-NA0003525. The Advanced Light Source is supported by the Director, Office of Science, Office of Basic Energy Sciences, of the U.S. Department of Energy under Contract No. DE-AC02-05CH11231. This paper describes objective technical results and analysis. Any subjective views or opinions that might be expressed in the paper do not necessarily represent the views of the USDOE or the United States Government.

9. Notes and References

1. Mansurov, Z. A., Soot Formation in Combustion Processes (Review). *Combust. Explos. Shock Waves*. 2005, 41 (6), 727.
2. Parker, D. S. N.; Kaiser, R. I.; Bandyopadhyay, B.; Kostko, O.; Troy, T. P.; Ahmed, M., Unexpected Chemistry from the Reaction of Naphthyl and Acetylene at Combustion-Like Temperatures. *Angew. Chem. Int. Ed.* 2015, 54 (18), 5421-5424.
3. Frenklach, M.; Wang, H., Detailed modeling of soot particle nucleation and growth. In *Symposium (International) on Combustion 1991* (Vol. 23, No. 1, pp. 1559-1566). Elsevier.
4. Mosbach, S.; Celnik, M. S.; Raj, A.; Kraft, M.; Zhang, H. R.; Kubo, S.; Kim, K. O., Towards a detailed soot model for internal combustion engines. *Combustion and Flame*. 2009; 156(6):1156-65.
5. Kaiser, R. I.; Parker, D. S. N.; Mebel, A. M., Reaction Dynamics in Astrochemistry: Low-Temperature Pathways to Polycyclic Aromatic Hydrocarbons in the Interstellar Medium. *Annu. Rev. Phys. Chem.* 2015, 66, 43-67.
6. McGuire, B. A.; Loomis, R. A.; Burkhardt, A. M.; Lee, K. L.; Shingledecker, C. N.; Charnley, S. B.; Cooke, I. R.; Cordiner, M. A.; Herbst, E.; Kalenskii, S.; Siebert, M. A., Detection of two interstellar polycyclic aromatic hydrocarbons via spectral matched filtering. *Science*. 2021; 371(6535):1265-9.
7. Sagan, C.; Khare, B. N.; Thompson, W. R.; McDonald, G. D.; Wing, M. R.; Bada, J. L.; Vo-Dinh, T.; Arakawa, E. T., Polycyclic aromatic hydrocarbons in the atmospheres of Titan and Jupiter. *The Astrophysical Journal*. 1993;414:399-405.
8. Mebel, A. M.; Georgievskii, Y.; Jasper, A. W.; Klippenstein, S. J., Pressure-dependent rate constants for PAH growth: formation of indene and its conversion to naphthalene. *Faraday discussions*. 2017;195:637-70.
9. Bauschlicher Jr CW, Ricca A. Mechanisms for polycyclic aromatic hydrocarbon (PAH) growth. *Chemical Physics Letters*. 2000;326(3-4):283-7.
10. Vander Wal, R. L.; Tomasek, A. J., Soot nanostructure: dependence upon synthesis conditions. *Combustion and Flame*. 2004;136(1-2):129-40.
11. Liu, P.; He, Z.; Hou, G. L.; Guan, B.; Lin, H.; Huang, Z., The diagnostics of laser-induced fluorescence (LIF) spectra of PAHs in flame with TD-DFT: special focus on five-membered ring. *The Journal of Physical Chemistry A*. 2015; 119(52):13009-17.
12. Vander Wal, R. L.; Tomasek, A. J., Soot oxidation: dependence upon initial nanostructure. *Combustion and flame*. 2003;134(1-2):1-9.

13. Parker, D. S. N.; Kaiser, R. I.; Troy, T. P.; Ahmed, M., Hydrogen Abstraction/Acetylene Addition Revealed. *Angew. Chem. Int. Ed.* 2014, 53 (30), 7740-7744.
14. Frenklach, M.; Mebel, A. M., On the mechanism of soot nucleation. *Phys. Chem. Chem. Phys.* 2020, 22 (9), 5314-5331.
15. Shukla, B.; Koshi, M., Comparative study on the growth mechanisms of PAHs. *Combustion and Flame*. 2011 Feb 1;158(2):369-75.
16. Andrae, J. C.; Brinck, T.; Kalghatgi, G. T., HCCI experiments with toluene reference fuels modeled by a semidetailed chemical kinetic model. *Combust Flame*. 2008, 1;155(4):696-712.
17. Zhang, L.; Cai, J.; Zhang, T.; Qi, F., Kinetic modeling study of toluene pyrolysis at low pressure. *Combust flame*. 2010, 1;157(9):1686-97.
18. Oehlschlaeger, M. A.; Davidson, D. F.; Hanson, R. K., Thermal decomposition of toluene: Overall rate and branching ratio. *Proc. Combust. Inst.* 2007, 1;31(1):211-9.
19. Klippenstein, S. J.; Harding, L. B.; Georgievskii, Y., On the formation and decomposition of C₇H₈. *Proc. Combust. Inst.* 2007, 1;31(1):221-9.
20. Eng, R. A.; Gebert, A.; Goos, E.; Hippler, H.; Kachiani, C., Incubation times, fall-off and branching ratios in the thermal decomposition of toluene: Experiments and theory. *Phys. Chem. Chem. Phys.* 2002 ;4(16):3989-96.
21. Buckingham, G. T.; Porterfield, J. P.; Kostko, O.; Troy, T. P.; Ahmed, M.; Robichaud, D. J.; Nimlos, M. R.; Daily, J. W.; Ellison, G. B., The thermal decomposition of the benzyl radical in a heated micro-reactor. II. Pyrolysis of the tropylium radical. *J. Chem. Phys.* 2016; 145(1):014305.
22. Shapero, M.; Cole-Filipiak, N. C.; Haibach-Morris, C.; Neumark, D. M., Benzyl radical photodissociation dynamics at 248 nm. *J. Phys. Chem. A*. 2015; 119(50):12349-56.
23. Dames, E.; Wang, H., Isomerization kinetics of benzylic and methylphenyl type radicals in single-ring aromatics. *Proc. Combust. Inst.* 2013; 34(1):307-14.
24. Seta, T.; Nakajima, M.; Miyoshi, A., High-temperature reactions of OH radicals with benzene and toluene. *J. Phys. Chem. A*. 2006;110(15):5081-90.
25. Li, Y.; Yuan, W.; Li, T.; Li, W.; Yang, J.; Qi, F., Experimental and kinetic modeling investigation of rich premixed toluene flames doped with n-butanol. *Phys. Chem. Chem. Phys.* 2018; 20(16):10628-36.
26. Tian, Z.; Pitz, W. J.; Fournet, R.; Glaude, P. A.; Battin-Leclerc, F., A detailed kinetic modeling study of toluene oxidation in a premixed laminar flame. *Proceedings of the Combustion Institute*. 2011; 33(1):233-41.
27. Yuan, W.; Li, Y.; Dagaut, P.; Yang, J.; Qi, F., Investigation on the pyrolysis and oxidation of toluene over a wide range conditions. II. A comprehensive kinetic modeling study. *Combust Flame*. 2015; 162(1):22-40.
28. Herbinet, O.; Husson, B.; Ferrari, M.; Glaude, P. A.; Battin-Leclerc, F., Low temperature oxidation of benzene and toluene in mixture with n-decane. *Proc. Combust. Inst.* 2013; 34(1):297-305.
29. Battin-Leclerc, F.; Bounaceur, R.; Belmekki, N.; Glaude, P. A., Experimental and modeling study of the oxidation of xylenes. *Int. J. Chem. Kinet.* 2006; 38(4):284-302.
30. Narayanaswamy, K.; Blanquart, G.; Pitsch, H., A consistent chemical mechanism for oxidation of substituted aromatic species. *Combust Flame*. 2010; 157(10):1879-98.
31. Mitra, T.; Chu, C.; Naseri, A.; Thomson, M. J., Polycyclic aromatic hydrocarbon formation in a flame of the alkylated aromatic trimethylbenzene compared to those of the alkane dodecane. *Combust. Flame*. 2021; 223:495-510.

32. Prendergast, M. B.; Cooper, P. A.; Kirk, B. B.; da Silva, G.; Blanksby, S. J.; Trevitt, A. J., Hydroxyl Radical Formation in the Gas Phase Oxidation of Distonic 2-Methylphenyl Radical Cations. *Phys. Chem. Chem. Phys.* 2013, 15, 20577-20584.
33. Prendergast, M. B.; Kirk, B. B.; Savee, J. D.; Osborn, D. L.; Taatjes, C. A.; Hemberger, P.; Blanksby, S. J.; da Silva, G.; Trevitt, A. J., Product detection study of the gas-phase oxidation of methylphenyl radicals using synchrotron photoionisation mass spectrometry. *Phys. Chem. Chem. Phys.* 2019, 21 (32), 17939-17949.
34. da Silva G, Chen CC, Bozzelli JW. Toluene combustion: reaction paths, thermochemical properties, and kinetic analysis for the methylphenyl radical+ O₂ reaction. *J. Phys. Chem. A*. 2007 Sep 6;111(35):8663-76.
35. Yang, T.; Parker, D. S. N.; Dangi, B. B.; Kaiser, R. I.; Mebel, A. M., Formation of 5- and 6-methyl-1H-indene (C₁₀H₁₀) via the reactions of the para-tolyl radical (C₆H₄CH₃) with allene (H₂CCCH₂) and methylacetylene (HCCCH₃) under single collision conditions. *Phys. Chem. Chem. Phys.* 2015, 17 (16), 10510-10519.
36. Parker, D. S. N.; Dangi, B. B.; Kaiser, R. I.; Jamal, A.; Ryazantsev, M. N.; Morokuma, K.; Korte, A.; Sander, W., An Experimental and Theoretical Study on the Formation of 2-Methylnaphthalene (C₁₁H₁₀/C₁₁H₃D₇) in the Reactions of the para-Tolyl (C₇H₇) and para-Tolyl-d₇ (C₇D₇) with Vinylacetylene (C₄H₄). *J. Phys. Chem. A* 2014, 118 (15), 2709-2718.
37. Yang, T.; Muzangwa, L.; Kaiser, R. I.; Jamal, A.; Morokuma, K., A combined crossed molecular beam and theoretical investigation of the reaction of the meta-tolyl radical with vinylacetylene - toward the formation of methylnaphthalenes. *Phys. Chem. Chem. Phys.* 2015, 17 (33), 21564-21575.
38. Thomas, A. M.; Yang, T.; Dangi, B. B.; Kaiser, R. I.; Kim, G. S.; Mebel, A. M., Oxidation of the para-Tolyl Radical by Molecular Oxygen under Single-Collision Conditions: Formation of the para-Toloxyl Radical. *J. Phys. Chem. Lett.* 2016; 7(24):5121-7.
39. Osborn, D. L.; Zou, P.; Johnsen, H.; Hayden, C. C.; Taatjes, C. A.; Knyazev, V. D.; North, S. W.; Peterka, D. S.; Ahmed, M.; Leone, S. R., The multiplexed chemical kinetic photoionization mass spectrometer: A new approach to isomer-resolved chemical kinetics. *Rev. Sci. Instrum.* 2008, 79 (10), 104103.
40. Savee, J. D.; Soorkia, S.; Welz, O.; Selby, T. M.; Taatjes, C. A.; Osborn, D. L., Absolute photoionization cross-section of the propargyl radical. *J. Chem. Phys.* 2012, 136 (13), 134307.
41. Suits, A. G.; Heimann, P.; Yang, X.; Evans, M.; Hsu, C. W.; Lu, K. t.; Lee, Y. T.; Kung, A. H., A differentially pumped harmonic filter on the Chemical Dynamics Beamline at the Advanced Light Source. *Rev. Sci. Instrum.* 1995, 66 (10), 4841-4844.
42. Heimann, P. A.; Koike, M.; Hsu, C. W.; Blank, D.; Yang, X. M.; Suits, A. G.; Lee, Y. T.; Evans, M.; Ng, C. Y.; Flaim, C.; Padmore, H. A., Performance of the vacuum ultraviolet high-resolution and high-flux beamline for chemical dynamics studies at the Advanced Light Source. *Rev. Sci. Instrum.* 1997, 68 (5), 1945-1951.
43. Leone, S. R.; Ahmed, M.; Wilson, K. R., Chemical dynamics, molecular energetics, and kinetics at the synchrotron. *Phys. Chem. Chem. Phys.* 2010, 12 (25), 6564-6578.
44. Stull, D. R., Vapor Pressure of Pure Substances. *Organic and Inorganic Compounds. Ind. Eng. Chem.* 1947, 39 (4), 517-540.
45. Frisch, M. J.; Trucks, G. W.; Schlegel, H. B.; Scuseria, G. E.; Robb, M. A.; Cheeseman, J. R.; Scalmani, G.; Barone, V.; Mennucci, B.; Petersson, G. A.; Nakatsuji, H.; Caricato, M.; Li, X.; Hratchian, H. P.; Izmaylov, A. F.; Bloino, J.; Zheng, G.; Sonnenberg, J. L.; Hada, M.; Ehara, M.; Toyota, K.; Fukuda, R.; Hasegawa, J.; Ishida, M.; Nakajima, T.; Honda, Y.; Kitao, O.; Nakai, H.;

- Vreven, T.; Montgomery, J. A.; Peralta, J. E.; Ogliaro, F.; Bearpark, M.; Heyd, J. J.; Brothers, E.; Kudin, K. N.; Staroverov, V. N.; Kobayashi, R.; Normand, J.; Raghavachari, K.; Rendell, A.; Burant, J. C.; Iyengar, S. S.; Tomasi, J.; Cossi, M.; Rega, N.; Millam, J. M.; Klene, M.; Knox, J. E.; Cross, J. B.; Bakken, V.; Adamo, C.; Jaramillo, J.; Gomperts, R.; Stratmann, R. E.; Yazyev, O.; Austin, A. J.; Cammi, R.; Pomelli, C.; Ochterski, J. W.; Martin, R. L.; Morokuma, K.; Zakrzewski, V. G.; Voth, G. A.; Salvador, P.; Dannenberg, J. J.; Dapprich, S.; Daniels, A. D.; Farkas, Ö.; Foresman, J. B.; Ortiz, J. V.; Cioslowski, J.; Fox, D. J., Gaussian 09 2009.
46. da Silva, G.; G3X-K theory: A composite theoretical method for thermochemical kinetics. *Chem. Phys. Lett.* 2013, 12;558:109-13.
 47. Zheng, J.; Zhao, Y.; Truhlar, D. G., The DBH24/08 Database and Its Use to Assess Electronic Structure Model Chemistries for Chemical Reaction Barrier Heights. *J. Chem. Theory Comput.* 2009, 5 (4), 808-821.
 48. Montgomery, J. A.; Frisch, M. J.; Ochterski, J. W.; Petersson, G. A., A complete basis set model chemistry. VI. Use of density functional geometries and frequencies. *J. Chem. Phys.* 1999, 110 (6), 2822-2827.
 49. Montgomery, J. A.; Frisch, M. J.; Ochterski, J. W.; Petersson, G. A., A complete basis set model chemistry. VII. Use of the minimum population localization method. *J. Chem. Phys.* 2000, 112 (15), 6532-6542.
 50. Fukui, K., The path of chemical reactions - The IRC approach. *Acc. Chem. Res.* 1981, 14 (12), 363-368.
 51. Barker, J. R.; Nguyen, T. L.; Stanton, J. F.; Aieta, C.; Ceotto, M.; Gabas, F.; Kumar, T. J. D.; Li, C. G. L.; Lohr, L. L.; Maranzana, A., MultiWell-2017 Software Suite; University of Michigan: Ann Arbor MI, 2017
 52. Barker, J. R., Multiple-Well, multiple-path unimolecular reaction systems. I. MultiWell computer program suite. *Int. J. Chem. Kinet.* 2001, 33, 232-245.
 53. Barker, J. R. Energy transfer in master equation simulations: A new approach. *Int. J. Chem. Kinet.* 2009, 41, 748-763.
 54. Eng, R. A.; Gebert, A.; Goos, E.; Hippler, H.; Kachiani, C., Incubation times, fall-off and branching ratios in the thermal decomposition of toluene: Experiments and theory. *Phys. Chem. Chem. Phys.* 2002; 4(16):3989-96.
 55. Vereecken, L.; Peeters, J., Reactions of chemically activated C₉H₉ species II: the reaction of phenyl radicals with allene and cyclopropene, and of benzyl radicals with acetylene. *Phys. Chem. Chem. Phys.* 2003; 5(13):2807-17.
 56. Vereecken, L.; Bettinger, H. F.; Peeters, J., Reactions of chemically activated C₉H₉ species. Part I. The product distribution of the reaction of phenyl radicals with propyne. *Phys. Chem. Chem. Phys.* 2002; 4(11):2019-27.
 57. Park, J.; Tokmakov, I. V.; Lin, M. C., Experimental and computational studies of the phenyl radical reaction with allene. *J. Phys. Chem. A.* 2007; 111(29):6881-9.
 58. McGlynn, S. P.; Rabalais, J. W.; McDonald, J. R.; Scherr, V. M., Electronic spectroscopy of isoelectronic molecules. II. Linear triatomic groupings containing sixteen valence electrons. *Chem. Rev.* 1971 Feb 1; 71(1):73-108.
 59. Miller, J. A.; Klippenstein, S. J., The recombination of propargyl radicals and other reactions on a C₆H₆ potential. *J. Phys. Chem. A.* 2003; 107(39):7783-99.
 60. Güsten, H.; Klasinc, L.; Rušćić, B., Photoelectron Spectroscopy of Heterocycles. Indene Analogs. In *Z. Naturforsch. A*, 1976; Vol. 31, pp 1051-1056.

61. Jochims, H. W.; Baumgärtel, H.; Leach, S., Structure-dependent photostability of polycyclic aromatic hydrocarbon cations: Laboratory studies and astrophysical implications. *Astrophys. J.* 1999; 512(1):500.
62. Dass, C.; Gross, M. L., Electrocyclic ring opening of 1-phenylcyclobutene and 3-phenylcyclobutene radical cations. *J. Am. Chem. Soc.* 1983; 105(18):5724-9.
63. Sebree, J. A.; Kislov, V. V.; Mebel, A. M.; Zwier, T. S., Isomer specific spectroscopy of C₁₀H_n, n= 8–12: Exploring pathways to naphthalene in Titan's atmosphere. *Faraday Discuss.* 2010, 147:231-49.
64. Dubnikova, F.; Lifshitz, A., Ring expansion and isomerization in methyl indene and methylene indene radicals. Quantum chemical and transition-state theory calculations. *Isr. J. Chem.* 2003; 43(3-4):325-38.
65. Koelsch, C. F.; Johnson, P. R., The Thermal Isomerization of Some Indene Derivatives. *J. Am. Chem. Soc.* 1943; 65(4):567-73.
66. Parker, D. D.; Zhang, D. F.; Kaiser, D. R.; Kislov, D. V.; Mebel, D. A., Indene Formation under Single-Collision Conditions from the Reaction of Phenyl Radicals with Allene and Methylacetylene—A Crossed Molecular Beam and Ab Initio Study. *Chem. Asian J.* 2011; 6(11):3035-47.
67. Vereecken, L.; Peeters, J.; Bettinger, H. F.; Kaiser, R. I.; Schleyer, P. V.; Schaefer, H. F., Reaction of phenyl radicals with propyne. *J. Am. Chem. Soc.* 2002; 124(11):2781-9.

TOC graphic

